Longitudinal evaluation of the biodistribution and cellular internalization of the bispecific CD3xTRP1 antibody in syngeneic mouse tumor models

Sandker, G.G.W.; Middelburg, J.; Wilbrink, E.; Molkenboer-Kuenen, J.; Aarntzen, E.; Hall, T. van; Heskamp, S.

Journal for ImmunoTherapy of Cancer

Longitudinal evaluation of the biodistribution and cellular internalization of the bispecific CD3xTRP1 antibody in syngeneic mouse tumor models

Gerwin Gerhard Wemke Sandker ,[1] Jim Middelburg,[2] Evienne Wilbrink,[1] Janneke Molkenboer-Kuenen,[1] Erik Aarntzen ,[1] Thorbald van Hall ,[2] Sandra Heskamp [1]

To cite: Sandker GGW, Middelburg J, Wilbrink E, *et al*. Longitudinal evaluation of the biodistribution and cellular internalization of the bispecific CD3xTRP1 antibody in syngeneic mouse tumor models. *Journal for ImmunoTherapy of Cancer* 2023;**11**:e007596. doi:10.1136/jitc-2023-007596

► Additional supplemental material is published online only. To view, please visit the journal online (http://dx.doi.org/10.1136/jitc-2023-007596).

Accepted 04 October 2023

[1]Department of Medical Imaging, Radboud University Medical Center, Nijmegen, The Netherlands
[2]Department of Medical Oncology, Oncode Institute, Leiden University Medical Center, Leiden, The Netherlands

Correspondence to
Prof. dr. Sandra Heskamp; Sandra.Heskamp@radboudumc.nl

ABSTRACT

Background CD3 bispecific antibodies (CD3-bsAbs) require binding of both a tumor-associated surface antigen and CD3 for their immunotherapeutic effect. Their efficacy is, therefore, influenced by the tumor uptake and the extracellular dose. To optimize their currently limited efficacy in solid tumors, increased understanding of their pharmacokinetics and in vivo internalization is needed.

Methods Here, were studied the pharmacokinetics and in vivo internalization of CD3xTRP1, a fully murine Fc-inert bsAb, in endogenous TRP1-expressing immunocompetent male C57BL/6J mice bearing TRP1-positive and negative tumors over time. Matching bsAbs lacking TRP1-binding or CD3-binding capacity served as controls. BsAbs were radiolabeled with ^{111}In to investigate their pharmacokinetics, target binding, and biodistribution through SPECT/CT imaging and ex vivo biodistribution analyses. Co-injection of ^{111}In- and ^{125}I-labeled bsAb was performed to investigate the in vivo internalization by comparing tissue concentrations of cellular residing ^{111}In versus effluxing ^{125}I. Antitumor therapy effects were evaluated by monitoring tumor growth and immunohistochemistry.

Results SPECT/CT and biodistribution analyses showed that CD3xTRP1 specifically targeted TRP1-positive tumors and CD3-rich lymphoid organ and uptake peaked 24 hours pi (KPC3-TRP1: 37.7%ID/g±5.3%ID/g, spleen: 29.0%ID/g±3.9%ID/g). Studies with control bsAbs demonstrated that uptake of CD3xTRP1 in TRP1-positive tumors and CD3-rich tissues was primarily receptor-mediated. Together with CD3xTRP1 in the circulation being mainly unattached, this indicates that CD3$^+$ T cells are generally not traffickers of CD3-bsAbs to the tumor. Additionally, target-mediated clearance by TRP1-expressing melanocytes was not observed. We further demonstrated rapid internalization of CD3xTRP1 in KPC3-TRP1 tumors (24 hours pi: 54.9%±2.3% internalized) and CD3-rich tissues (spleen, 24 hours pi: 79.7%±0.9% internalized). Therapeutic effects by CD3xTRP1 were observed for TRP1-positive tumors and consisted of high tumor influx of CD8$^+$ T cells and neutrophils, which corresponded with increased necrosis and growth delay.

Conclusions We show that CD3xTRP1 efficiently targets TRP1-positive tumors and CD3-rich tissues primarily through receptor-mediated targeting. We further demonstrate rapid receptor-mediated internalization of CD3xTRP1 in TRP1-positive tumors and CD3-rich tissues. Even though this significantly decreases the therapeutical available dose, CD3xTRP1 still induced effective antitumor

WHAT IS ALREADY KNOWN ON THIS TOPIC

⇒ In solid cancers, the efficacy of CD3-bsAbs is still limited, potentially because processes negatively affecting their pharmacokinetics can reduce the effective tumor targeted dose. These processes include "on-target, off-tumor" targeting, target-mediated clearance, and in vivo internalization.

WHAT THIS STUDY ADDS

⇒ In a fully immunocompetent and non-artificial syngeneic tumor mouse model setting we show efficient CD3xTRP1 bsAb uptake in TRP1-positive tumors and CD3-rich tissues and that the uptake is primarily receptor-mediated and not through trafficking by CD3$^+$ T cells.

⇒ Endogenous TRP1-expression by healthy tissues does not necessarily negatively affect CD3xTRP1's pharmacokinetics through target-mediated clearance.

⇒ Rapid internalization of CD3xTRP1 in TRP1-expressing tumors and CD3-rich tissues does not prevent effective induction of therapeutical responses.

HOW THIS STUDY MIGHT AFFECT RESEARCH, PRACTICE OR POLICY

⇒ Our data on the in vivo pharmacokinetics and mechanism of action of CD3xTRP1 bsAb indicate that methods to shift CD3-bsAb uptake from lymphoid tissues to the tumor and/or decreases its internalization could increase therapeutical available tumor targeted doses, this paves the way for further optimization of CD3-bsAb therapy for solid tumors.

T-cell responses and inhibited tumor growth. Together, our data on the pharmacokinetics and mechanism of action of CD3xTRP1 pave the way for further optimization of CD3-bsAb therapies.

INTRODUCTION

Immunotherapeutic CD3-targeting bispecific antibodies (CD3-bsAbs) show therapeutic potential in a multitude of malignancies.[1] These bsAbs are designed to specifically bind CD3 and a tumor-associated surface antigen (TAA). On simultaneous binding to CD3 and the TAA, an immunological synapse is formed, resulting in local T-cell activation and tumor-cell killing independent of TCR specificity, and thus elicits antitumor activity even from non-tumor-specific T cells.[2]

CD3-bsAbs have shown impressive clinical results for hematological malignancies.[3 4] In solid cancers, however, their therapeutic efficacy is still limited for several reasons. First, their immunosuppressive tumor microenvironment is characterized by poor infiltration and reduced effector T-cell function.[5] Second, poor vascularization and low or heterogeneous TAA expression may hamper CD3-bsAbs tumor accumulation.[6] Third, expression of TAAs on healthy tissues potentially affects pharmacokinetics (PK) and biodistributions of CD3-bsAbs through target-mediated clearance. Furthermore, it increases the potential for adverse effects through "on-target, off-tumor" binding.[7] Thus, factors affecting tumor uptake and PK play an important role CD3-bsAbs' efficacy and toxicity profiles, especially for solid tumors.[8] Additionally, as the binding of CD3-bsAbs to both the TAA and CD3 on the cell membrane is required to induce the formation of the cytolytic synapse, its extracellular localization is essential for eliciting antitumor T-cell responses. Internalization of CD3-bsAbs consequently negates their therapeutic potential. Therefore, thorough understanding of CD3-bsAbs' PK and in vivo cellular internalization is essential to increase efficacy of novel CD3-bsAbs for solid cancers.

Nuclear imaging of radiolabeled CD3-bsAbs allows for evaluating their PK and biodistribution on a full-body scale. Preclinical models enable detailed translational studies to investigate more complex characteristics, such as in vivo internalization. As preclinical studies with human CD3-bsAbs are restricted to immunodeficient or artificial models because they lack cross-species specificity, they omit the complex immunological interplay of CD3-bsAbs with their targets. Although human CD3 and human TAA knock-in models resolve most of these obstacles, they usually express the proteins at higher levels compared with endogenous expression. Furthermore, their use is only practicable when the TAAs function is not (severely) altered and they might not account for factors such as, steric hinderance.[9] Moreover, protection against the generation of anti-IgG antibodies which can affect the human CD3-bsAbs' biodistribution is not guaranteed. Thus, the use of artificial models can considerably complicate the translation of biodistribution results to the clinical setting. Therefore, we investigated the PK, biodistribution, and in vivo internalization of a fully murine Fc-inert bsAb targeting murine CD3ε and murine tyrosinase-related protein 1 (TRP1, also gp75 or TYRP-1) (CD3xTRP1 bsAb) that has been extensively evaluated for its immunological effects.[10 11] TRP1 is translationally of interest as it is similarly expressed in mice and humans, with endogenous expression on melanocytes and upregulated expression in melanomas. The human analog of CD3xTRP1 is currently investigated in clinical trials.[12 13]

Here, we report the PK, biodistribution, and in vivo internalization of radiolabeled CD3xTRP1 bsAb and control bsAbs in fully syngeneic tumor mouse models with endogenous TRP1 expression. We show that CD3xTRP1 specifically accumulates in TRP1 expressing tumors and CD3-rich tissues. Furthermore, effective antitumor immune responses were induced, even though rapid bsAb internalization in TRP1 expressing tumors and secondary lymphoid organs occurred.

METHODS

Cell culture

KPC3 murine pancreatic ductal adenocarcinoma cells (further KPC3) were transfected to express TRP1 (KPC3-TRP1), whereas B16F10 murine melanoma cells (CRL6475, ATCC) endogenously express TRP1 at approximately a five-fold lower level than KPC3-TRP1.[10 14] KPC3-TRP1, KPC3, and B16F10 cells were cultured in Iscove's Modified Dulbecco's Medium (IMDM, Gibco) supplemented with L-glutamine, 25 mM HEPES, and 8% fetal calf serum (FCS, Sigma-Aldrich Chemie BV). TK-1 murine T-cell lymphoma cells (CRL-2396, ATCC) were cultured in Dulbecco's Modified Eagle Medium high glucose (DMEM GlutaMAX, Gibco) supplemented with 1 mM pyruvate (Gibco) and 10% FCS. All cells were cultured at 37°C in a humidified atmosphere with 5% CO_2. Cells were tested and found negative for mycoplasma and mouse pathogens.

BsAbs and radiolabeling

Fc-γ effector-function silenced IgG2a bsAb CD3xTRP1 (2C11 and TA99 arms with dissociation constants of 22.0 and 1.5 nM, respectively[15–18]), and control CD3xMock and TRP1xMock whose TRP1 or CD3-arm was replaced with non-relevant influenzavirus-specific "Mock" arms (B12[19]), were previously produced and provided by Genmab.[11] BsAbs were conjugated with a 15-fold molar excess of isothiocyanatobenzyl-diethylenetriaminepentaacetic acid (ICT-DTPA, p-SCN-Bn-DTPA, Macrocyclics) in 0.1 M $NaHCO_3$ (pH 9.5), for 1 hour at RT. To evaluate the conjugation ratio, samples were radiolabeled with $^{111}InCl_3$ (Curium) at low specific activity (A_s:0.3 MBq/µg) in 0.5 M MES buffer (pH 5.4) for 15–20 min at RT. Subsequently, we performed instant thin-layer chromatography (iTLC), using silica gel chromatography strips (Agilent Technologies) and 0.1 M, pH 6.0 citrate (Sigma-Aldrich) as running buffer. The iTLC activity profiles were analyzed for the two fractions: (1) ^{111}In-chelated

by DTPA-bsAb and (2) ^{111}In-chelated by unconjugated DTPA, using photosensitive plates (Fuji MS, Cytiva), a phosphor imager (Typhoon FLA 7000, GE), and AIDA software V.4.21.033 (Raytest, Straubenhardt). Conjugation ratios were calculated by multiplying the fraction of ^{111}In-labeled to DTPA-bsAb with the starting molar ratio of DTPA:antibody. Conjugation ratios of DTPA:antibody were 1.6, 1.6, and 1.4 for CD3xTRP1, CD3xMock, and TRP1xMock, respectively. Next, unreacted ITC-DTPA was removed from the conjugation mixture by dialysis against 0.25 M ammonium acetate (NH_4Ac, pH 5.4–5.5, metal free) supplemented with 2 g/L Chelex (Bio-Rad) using 20,000 molecular weight cut-off dialysis cassettes (Slide-a-Lyzer, Thermofisher).

DTPA-bsAbs were radiolabeled with $^{111}InCl_3$ as described above. Next, unincorporated ^{111}In was chelated by adding EDTA in phosphate-buffered saline (PBS) to a final 5 mM concentration. Iodine-125 (^{125}I) labeling was performed by incubating DTPA-bsAbs in iodogen coated Eppendorf tubes with $Na^{125}I$ (10^{-5} M NaOH, Perkin Elmer) in 0.5 M phosphate buffer (pH 7.4) with the total reaction volume adjusted to 100 µL with H_2O, for 10 min at RT. The reaction was quenched with a saturated tyrosine solution. Labeling efficiencies were evaluated with iTLC as described above and were >95% for in vivo and >90% for in vitro experiments. Labeled products were used without further purification. For in vivo experiments, the reaction mixture was adjusted to pH 7.4 with 10x PBS (pH 7.4). Unlabeled bsAb and sterile pyrogen-free PBS were added to reach a final concentration of 62.5 µg/mL.

In vitro characterization

The purity and stability of the radiolabeled antibodies were assessed with high-performance liquid chromatography (HPLC) and iTLC, respectively. We evaluated whether DTPA-conjugation and radiolabeling affected CD3- or TRP1-binding of CD3xTRP1 and control bsAbs with flow cytometry, lactate dehydrogenase (LDH) cytotoxicity, and in vitro binding assays.

HPLC quality control

BsAbs were ^{111}In-labeled as described above (A_s: 0.5 MBq/µg) and additional unlabeled bsAb was added to increase the protein detectability. We performed HPLC (LC-2030C, Shimadzu) using an SEC-3000 column (00 H-4513-K0, Phenomenex), which was eluted with a mobile phase of 0.1 M Na_3PO_4, 0.1 M Na_2SO_4, and 10% isopropanol at a flow rate: 0.7 mL/min. UV and radio signal-detectors measured at 280±4 nm and 100–300 keV, respectively. Data was analyzed using SARA v10.4 (Elysia-Raytest). The only two observed UV peaks coincided with the two activity peaks and showed expected retention times for antibodies (11.13, 11.25, and 11.28 min) and EDTA (16.45, 16.47, and 16.48 min) (online supplemental figure S1). No impurities were observed.

Stability test

The stability of radiolabeled (^{111}In and ^{125}I) bsAbs was analyzed over time. After radiolabeling (A_s: 0.5 MBq/µg), the reaction mixture was purified using a buffer exchange column (PD-10, Cytiva) using PBS supplemented with 0.5% bovine serum albumin (BSA). Next, 1/10th volume of 1% Tween80 in PBS/0.5%BSA was added and 160 µL was transferred in triplicate to a lobind Eppendorf tube. Samples were kept at 4°C and iTLC was performed as described above at 0, 24, 72, and 168 hours.

Flow cytometry

KPC3, KPC3-TRP1, and TRP1-positive B16F10 cells were stained with 10 µg/mL unconjugated CD3xTRP1 or DTPA-conjugated CD3xTRP1 in PBS supplemented with 0.5% BSA (Sigma) and 0.002% sodium azide (FACS buffer) for 20 min at 4°C. Next, cells were washed with FACS buffer and stained with goat-anti-mouse IgG-Alexa Fluor647 (1:400, Biolegend) in FACS buffer for 20 min at 4°C. Finally, cells were resuspended in FACS buffer, measured on a flow cytometer (LSRFortessa X-20, BD bioscience), and analyzed with FlowJo V.10.8.1 (Treestar).

LDH cytotoxicity assay

Proliferation of KPC3 and KPC3-TRP1 was arrested by irradiation with 6000 Rad (Gammacell 1000 Elite, Best Theratronics). Subsequently, 30,000 tumor cells/well were seeded in 96-well plates and allowed to adhere for 4 hours. T cells were isolated from spleens of naïve C57BL/6J mice using nylon wool fiber columns to remove B cells. Then, 300 000 T cells/well and either non-conjugated or DTPA-conjugated CD3xTRP1 bsAbs was added and incubated for 2 days at 37°C. Tumor cell killing was assessed using the CyQUANT LDH cytotoxicity assay (Thermo Fisher) following the manufacturers protocol. Absorbance was measured on a Spectramax iD5 plate-reader (Molecular Devices). The percentage of cytotoxicity was calculated, after correcting for absorbance of medium only and tumor cell only controls, from the absorbance of the treated samples and Triton100-lysed maximum kill control samples.

In vitro binding assay

KPC3-TRP1 (1.4×10^6 cells/mL), KPC3 (1.4×10^6 cells/mL), and B16F10 (1.4×10^6 cells/mL) cells were resuspended in IMDM/0.5%BSA, and TK-1 (4.0×10^6 cells/mL) cells in DMEM/0.5%BSA, and incubated with equimolar concentrations (0.75 pM) of [^{111}In]In-CD3xTRP1 (A_s: 3.8 MBq/µg, 0.85 kBq) or [^{125}I]I-CD3xTRP1 (A_s: 3.1 MBq/µg, 0.7 kBq) for 3.5 hours at 37°C. Cells were washed twice and cell-associated activity was subsequently measured in a well-type gamma-counter (Wallac 2480 wizard, Perkin Elmer). In a separate binding assay equimolar concentrations (1.97 pM) of [^{111}In]In-CD3xMock (A_s: 1.28 MBq/µg, 0.76 kBq) and [^{111}In]In-TRP1xMock (A_s: 1.26 MBq/µg, 0.75 kBq) were incubated with KPC3-TRP1 (0.8×10^6 cells/mL), KPC3 (2.6×10^6 cells/mL), or TK-1 (8.5×10^6 cells/mL) in RPMI-1640/0.5%BSA (Gibco) for

40 min at 37°C. Cell-associated activity was measured as described above.

Animal studies

Male C57BL/6J mice (n=78, 6–8 weeks, Charles River, Germany) were housed under specific-pathogen-free conditions in individually ventilated cages with a filter top (Green line IVC, Tecniplast), in the presence of cage enrichment with food and water ad libitum. For tumor inoculation, mice were injected subcutaneously with 200 µL PBS/0.1%BSA containing; (1) 0.8×10^5 KPC3-TRP1 cells (right flank) and 0.8×10^5 KPC3 cells (left flank), or 2) 0.8×10^5 B16F10 cells (right flank). Tumor size was measured using a caliper twice weekly. KPC3 and KPC3-TRP1 tumor-bearing mice were block-randomized based on tumor size and injected with radiolabeled bsAbs 17 days after inoculation. B16F10 tumor-bearing mice received [^{111}In]In-CD3xTRP1 8 days post inoculation. Confounding effects of cage allocation were prevented by pooling mice from different groups. Humane endpoints were based on the general level of discomfort and tumor sizes; animal health was checked daily. Researchers and biotechnicians were blinded for group allocation.

Ex vivo biodistribution analyses

To assess the pharmacokinetics, biodistribution, and therapeutic availability of CD3xTRP1 we performed ex vivo biodistribution experiments with ^{111}In- and ^{125}I-labeled CD3xTRP1, CD3xMock, and TRP1xMock in KPC3 and KPC3-TRP1 tumor-bearing mice at several time points. Mice (n=7/group) were injected intraperitoneally in the right caudal abdomen with 200 µL PBS/0.1%BSA containing 12.5 µg of a 1:1 mixture of ^{111}In- and ^{125}I-labeled; a) CD3xTRP1 ([^{111}In]In and [^{125}I]I, A_s: 0.069 and 0.027 MBq/µg, 0.43 and 0.17 MBq, (n=21)), b) CD3xMock (A_s: 0.070 and 0.027 MBq/µg, 0.44 and 0.17 MBq, (n=21)), or c) TRP1xMock (A_s: 0.069 and 0.027 MBq/µg, 0.43 and 0.17 MBq, (n=21)). At 24, 72, or 168 hours post injection (pi), mice were euthanized by CO_2/O_2 asphyxiation, blood was collected via heart puncture and relevant tissues (blood, muscle, shaven pigmented skin, shaven non-pigmented skin, right and left inguinal lymph nodes, tumors, spleen, thymus, bone marrow, bone, pancreas, duodenum, heart, lung, kidney, liver, stomach, colon, brown adipose tissue, prostate) were collected for biodistribution analysis. To separate the serum and cell pellet, blood was stored in an Eppendorf tube for 30 min at RT, followed by centrifugation at 2000 g for 10 min at 4°C. Tissue and blood samples were weighed (XPE105DR, Mettler Toledo) and radioactivity concentrations were measured with a well-type gamma-counter. Aliquots of injection fluid served as reference controls. Tissue accumulation of [^{111}In]In-bsAb and [^{125}I]I-bsAb was calculated as a percentage of the injected dose (%ID) and normalized for tissue weight (percentage injected dose per gram (%ID/g)). To evaluate the absolute accumulated dose in the tumors, spleen, and lymph nodes, we calculated the %ID accumulated in the entire tissue. In vivo internalization of bsAbs was investigated by evaluating ^{125}I-to-^{111}In ratios of tissue uptake concentrations; on internalization and subsequent degradation ^{125}I effluxes from the cell,[20] whereas ^{111}In resides intracellularly.[21] Tumor tissues were fixated in PBS/4%formalin for immunohistochemical (IHC) analysis.

SPECT/CT imaging

To longitudinally visualize the in vivo biodistribution of CD3xTRP1 and control bsAbs in KPC3 and KPC3-TRP1 tumor-bearing and B16F10 tumor-bearing mice, we performed single-photon emission computed tomography (SPECT)/computed tomography (CT) imaging at various time points. KPC3 and KPC3-TRP1 tumor-bearing mice (n=3/group) were injected intraperitoneally in the right caudal abdomen with 12.5 µg [^{111}In]In-CD3xTRP1, [^{111}In]In-CD3xMock, or [^{111}In]In-TRP1xMock (A_s: 1.49, 1.53, and 1.45 MBq/µg, 15.4–17.7 MBq). SPECT/CT (U-SPECT II/CT, MILabs) images were acquired at 6, 24, and 72 hours pi (acquisition times: 15, 25, and 35 min, respectively), under inhalation anesthesia (2% isoflurane in air) on a heated bed (38°C), and 168 hours pi following CO_2/O_2 asphyxiation (acquisition time: 55 min), using a 1.0 mm diameter pinhole mouse collimator, and CT parameters of 160 µm spatial resolution, 615 µA, and 65 kV. Data were reconstructed with MILabs software v2.04 using the following settings: energy windows at 171 keV (154–188 keV) and 245 keV (220–270 keV), 1 iteration, 16 subsets and a 0.2 mm voxel size. We used Inveon Research Workplace software v4.2 to create maximum-intensity projections after applying a gaussian 2×2×2 voxel filter. In a separate experiment, B16F10 tumor-bearing mice (n=6) were injected intraperitoneally in the right caudal abdomen with 12.5 µg [^{111}In]In-CD3xTRP1 (A_s: 1.47 MBq/µg, 14.2–14.5 MBq), followed by SPECT/CT imaging at 24 hours pi under inhalation anesthesia (2% isoflurane in air) and 72 hours pi following CO_2/O_2 asphyxiation, using the same acquisition parameters as described above. After SPECT/CT, ex vivo biodistribution analyses (without serum analysis) were performed as described above.

Immunohistochemistry

Consecutive KPC3 and KPC3-TRP1 tumor sections (5 µm) were evaluated for CD3, CD8, Ly6G, F4/80, PD-L1, and H&E. The staining-procedure for H&E, Ly6G, F4/80, PD-L1 were described previously.[22] For CD8 and CD3, sections were deparaffinized and rehydrated, followed by antigen retrieval in 1× Tris, Borate, EDTA buffer (Amresco/VWR, pH 8.3) containing 0.05% Tween-20 at 96°C for 10 min. Then, endogenous peroxidases, endogenous biotin, and non-specific Ig binding were blocked using 3% H_2O_2, a biotin/avidin blocking set (SP-2001, Vector), and normal goat serum (5095, Bodinco), respectively. Primary antibody rabbit-anti-mouse CD8alpha (1:4,000, ab209775, Abcam) was incubated overnight at 4°C, and rabbit-anti-mouse CD3 (1:400, ab16669, Abcam) for 60 min at RT. Next, secondary antibody

goat-anti-rabbit/biotin antibody (1:200, BA-1000, Vector) was incubated for 30 min at RT. Thereafter, for signal amplification, sections were incubated with horseradish peroxidase-Biotin/Streptavidin Complex (1:100, PK-6100, Vectastain) for 30 min at RT. Finally, sections were incubated with bright 3,3'-diaminobenzidine (DAB, B-500, Immunologic) for 8 min, counterstained with hematoxylin (Klinipath/VWR), dehydrated, and mounted with a cover slip using permount (Fisher). Sections were analyzed with blinding for group allocation. Representative tumors sections (n=3/group) were selected by visual scoring and scanned at ×20 magnification using a Pannoramic 1000 (0.242535×0.242647 µm/pixel, 3DHISCTECH). Images were created from representative tumor areas using Caseviewer v2.3. Intratumoral $CD3^+$ and $CD8^+$ T-cell presence was quantified on images (n=3 mice/group, n=6 images/section) at ×10 magnification in Fiji V.1.53t using; color deconvolution (H DAB), auto threshold "Yen", and analyze particles (size=10 to 400) to calculate the %DAB-stained area.

Statistical analyses

The required number of animals was determined by a priori sample size calculations for KPC3-TRP1 tumor uptake based on previously obtained data. 11 mice were excluded from analysis: (1) one B16F10 tumor did not develop, (2) one B16F10 tumor-bearing and nine KPC3 and KPC3-TRP1 tumor-bearing mice from various groups were misinjected intraperitoneally, which was posteriorly defined as an [^{111}In]In-bsAb blood level ≤1/5th of the groups mean at time of dissection. All results are presented as mean±SD, unless stated otherwise. Differences in [^{111}In]In-bsAbs' blood concentrations and tissue uptake was tested for significance using two-way analysis of variances (ANOVAs) with Bonferroni post hoc tests. Differences in KPC3 and KPC3-TRP1 tumor volumes, and increases of intratumoral $CD3^+$ and $CD8^+$ T cells of CD3xTRP1 or control treated mice were tested for statistical significance using one-way ANOVAs with Bonferroni post hoc tests and two-tailed t-tests, respectively. Statistical significance was defined as $p \leq 0.05$ and tests were performed with GraphPad Prism V.9.5.

RESULTS

CD3xTRP1 target binding is unaffected by radiochemical procedures

To assess whether bsAb conjugation with the (radio)metal chelator DTPA and/or radiolabeling affected CD3- or TRP1-binding, we performed flow cytometry, LDH cytotoxicity, and in vitro binding assays. Flow-cytometric analysis of equimolar concentrations showed similar binding of unconjugated CD3xTRP1 and DTPA-CD3xTRP1 to both KPC3-TRP1 and TRP1-expressing B16F10 cells, while no binding was observed to TRP1-negative KPC3 cells (figure 1A). Furthermore, it showed that TRP1 expression levels were approximately fivefold higher on KPC3-TRP1 compared with B16F10 cells. In addition, the LDH cell killing assay showed equal induction of cytotoxicity of naïve splenic T cells to KPC3-TRP1 cells by DTPA-conjugated CD3xTRP1 and unconjugated CD3xTRP1 at all tested doses (figure 1B). Moreover, both ^{111}In- and ^{125}I-labeled DTPA-CD3xTRP1 showed specific binding to TRP1 and CD3, which was not significantly different from each other (figure 1C). Target binding of [^{111}In]In-CD3xMock to CD3 and [^{111}In]In-TRP1xMock to TRP1 was also confirmed (figure 1D). Stability assays showed minimal release (<1%) of ^{111}In and ^{125}I from the radiolabeled antibodies up to 168 hours after radiolabeling (online supplemental figure S2). Taken together, ITC-DTPA conjugation and radiolabeling of CD3xTRP1 did not interfere with target binding and T-cell activation.

CD3xTRP1 distribution is mediated via both the CD3- and TRP1-binding arm

We evaluated in vivo target specificity of the CD3- and TRP1-binding arms with SPECT/CT and ex vivo biodistribution studies using ^{111}In-labeled CD3xTRP1 and control bsAbs lacking either the CD3-binding or TRP1-binding arm. SPECT/CT revealed [^{111}In]In-CD3xTRP1 accumulation in CD3-rich tissues and KPC3-TRP1 tumors and not in parental KPC3 tumors. [^{111}In]In-CD3xMock merely distributed to CD3-rich tissues and not to KPC3-TRP1 tumors (figures 2 and 3), while [^{111}In]In-TRP1xMock uptake was only observed in KPC3-TRP1 tumors. These results indicate that CD3xTRP1 tissue uptake is target mediated. Additionally, SPECT/CT imaging showed accumulation of all three bsAbs in the peri- and extratumoral region extending caudally toward the hip of both KPC3-TRP1 and KPC3 tumors (figures 2 and 3), indicating a non-CD3 and non-TRP1 mediated process. Moreover, in B16F10 tumor-bearing mice this accumulation was not observed, suggesting a tumor model specific process (figure 3A,B).

Biodistribution analyses quantitatively confirmed these results; uptake of [^{111}In]In-TRP1xMock in KPC3-TRP1 tumors was significantly higher compared with [^{111}In]In-CD3xTRP1 (72 hours pi: 74.2%ID/g±15.4%ID/g vs 33.5%ID/g±15.4%ID/g, $p<0.001$), whereas its uptake in CD3-rich tissues, such as the spleen, was significantly lower (online supplemental figure S2 and table S1). Inversely, uptake of [^{111}In]In-CD3xMock in KPC3-TRP1 tumors was significantly lower compared with bsAbs with a TRP binding arm, while uptake in CD3-rich organs was significantly higher (spleen 72 hours pi, CD3xMock vs CD3xTRP1: 46.4%ID/g±17.7%ID/g vs 23.8%ID/g±10.4%ID/g, $p<0.001$). Additionally, this suggests that KPC3-TRP1 and secondary lymphoid organ uptake of CD3xTRP1 was not saturated. Blood levels and marker negative tissue uptake were unaffected by removal of CD3- or TRP1-binding capacity. In pigmented and non-pigmented skin [^{111}In]In-CD3xTRP1 uptake was not statistically significant different. Additionally, it was comparable to skin uptake of CD3xMock and TRP1xMock (online supplemental table S1). This indicated no pronounced specific uptake of CD3xTRP1 in healthy

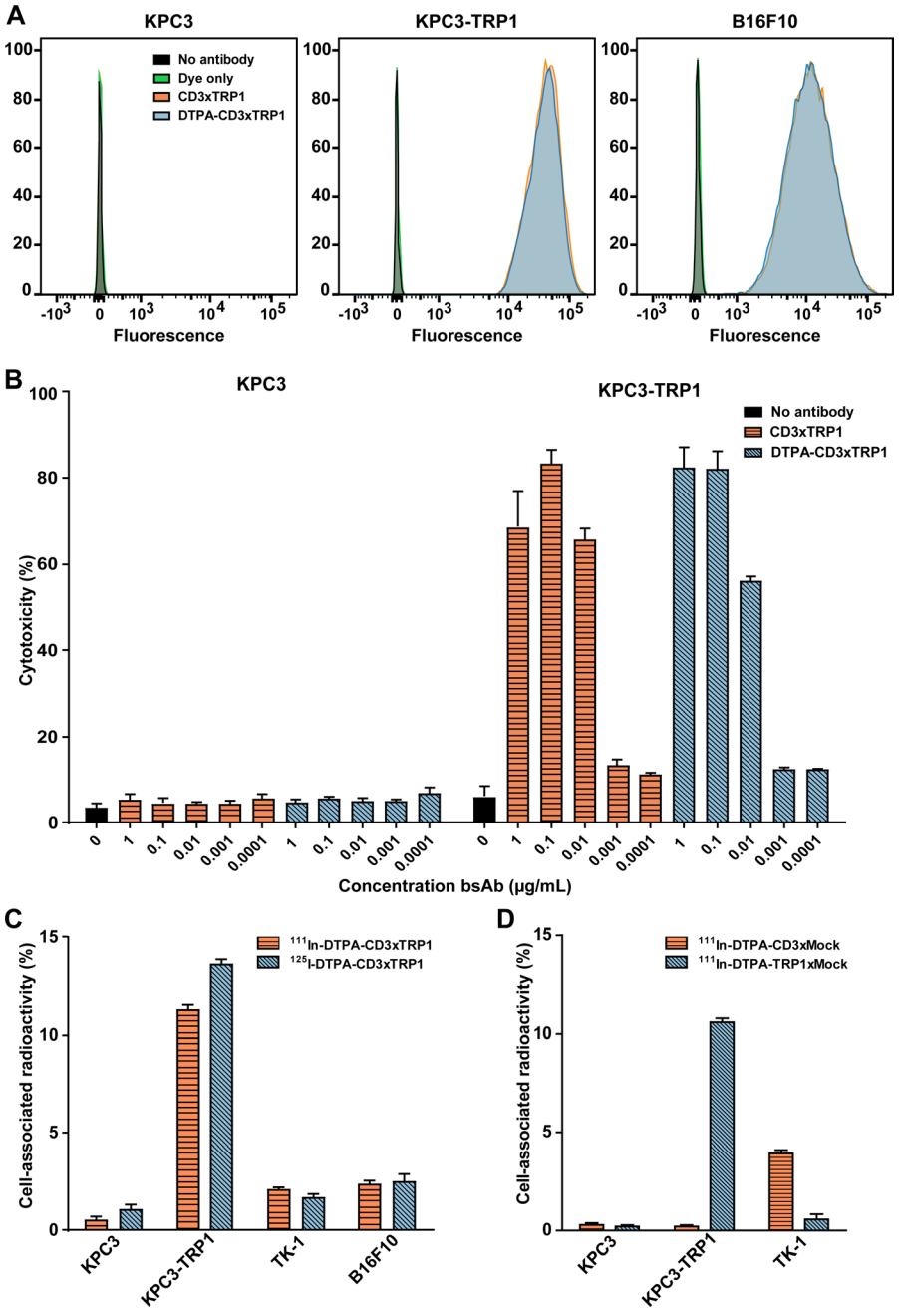

Figure 1 In vitro evaluation of cell binding and cytotoxicity of CD3xTRP1 after DTPA-conjugation and radiolabeling. (A) Flow cytometry analysis of unconjugated and DTPA-conjugated CD3xTRP1 target binding on KPC3, KPC3-TRP1, and TRP1-positive B16F10 cells. (B) LDH cytotoxicity assay on KPC3 and KPC3-TRP1 cells with unconjugated or DTPA-conjugated CD3xTRP1. (C) Binding assays of [^{111}In]In-CD3xTRP1 and [^{125}I]I-CD3xTRP1 on KPC3, KPC3-TRP1, CD3-positive TK-1, and TRP1-positive B16F10 cells. (D) Binding assays of [^{111}In]In-CD3xMock and [^{111}In]In-TRP1xMock on KPC3, KPC3-TRP1, and CD3^{+} Tk-1 cell lines. LDH, lactate dehydrogenase.

pigmented skin. In summary, SPECT/CT imaging and biodistribution analyses showed CD3-specificity and TRP1-specificity of CD3xTRP1.

CD3xTRP1 efficiently targets tumors expressing TRP1

To investigate the in vivo distribution of CD3xTRP1 over time, we evaluated the pharmacokinetics of [^{111}In]In-CD3xTRP1 in C57BL/6J mice bearing: (1) KPC3 and KPC3-TRP1 tumors and (2) B16F10 tumors. CD3xTRP1 blood levels were highest at 24 hours pi and decreased gradually over time (figure 3). KPC3-TRP1 tumor uptake was highest at 24 hours pi (37.7%ID/g±5.3%ID/g) and steadily decreased thereafter (168 hours: 15.1%ID/g±5.8%ID/g, p<0.001), but was significantly higher compared with KPC3 tumor uptake (168 hours: 3.3%ID/g±1.5%ID/g, p<0.05). Spleen, lymph node, and bone marrow showed similar trends with CD3xTRP1 uptake peaking 24 hours pi, whereas thymic uptake peaked at 72 hours pi. For a comprehensive overview of the

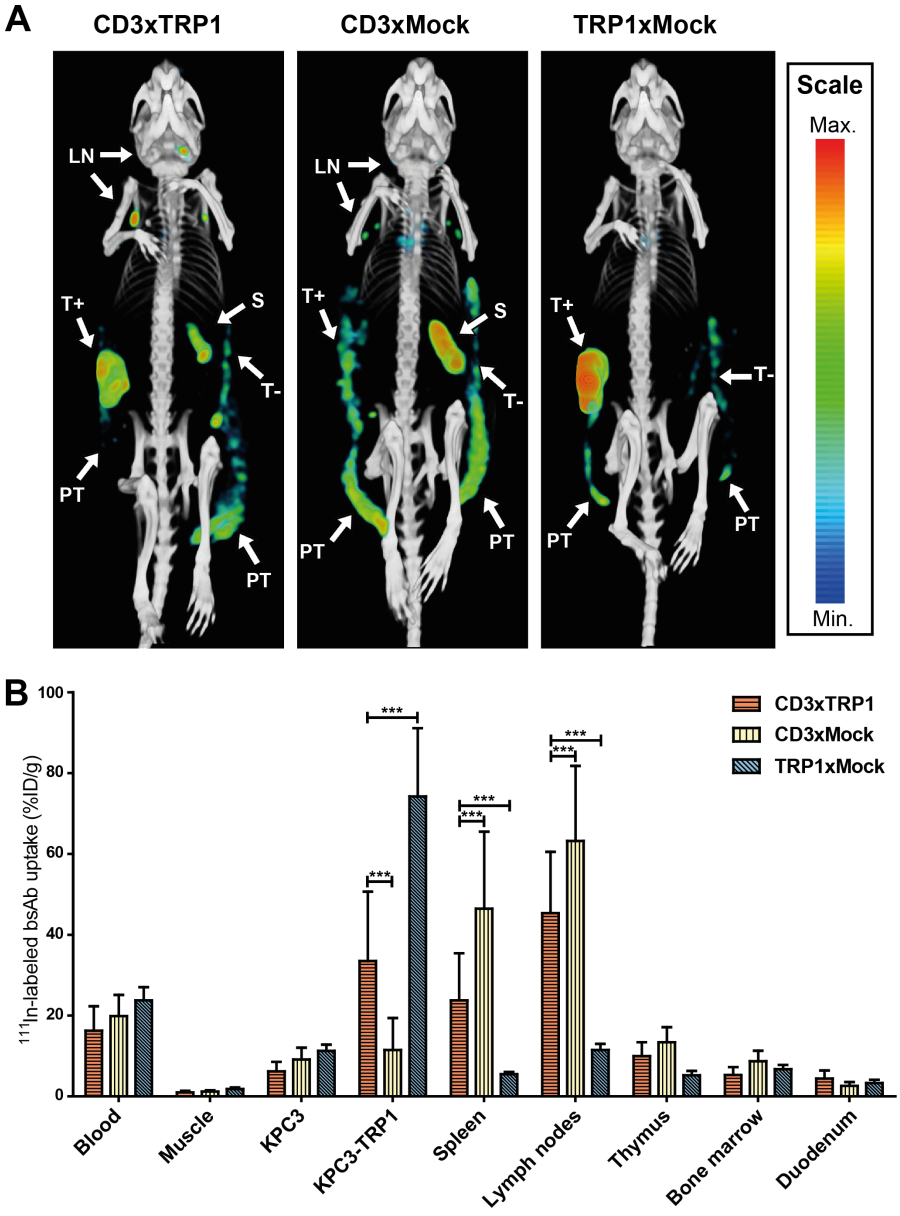

Figure 2 In vivo biodistribution of CD3xTRP1, CD3xMock, and TRP1xMock. MicroSPECT/CT and ex vivo biodistribution analysis of 12.5 µg [^{111}In]In-CD3xTRP1, [^{111}In]In-CD3xMock, and [^{111}In]In-TRP1xMock in C57BL/6J mice bearing KPC3 and KPC3-TRP1 tumors on contralateral flanks, 72 hours post intraperitoneal injection. (A) In vivo biodistribution of [^{111}In]In-bsAbs visualized with MIPs generated from microSPECT/CT data using the same thresholds at time point. Indicated tissues with [^{111}In]In-bsAbs uptake: KPC3-TRP1 tumor (T+), KPC3 tumor (T-), spleen (S), lymph nodes (LN), and peritumoral and extratumoral accumulation (PT). (B) Ex vivo biodistribution analysis of [^{111}In]In-bsAbs. Only relevant tissues are depicted. Tissue uptake is presented as %ID/g, differences in uptake were tested for significance using two-way ANOVAs with a Bonferroni post hoc test (***p<0.001). ANOVA, analysis of variance; %ID, percentage of the injected dose.

biodistributions see online supplemental table S1. As tumor growth continued after bsAb injection, the weight-corrected uptake concentrations decreased. In terms of absolute tumor uptake (%ID) we observed that CD3xTRP1 in KPC3-TRP1 tumors was constant over time. Thus, the decreased tumor uptake concentrations were likely a result of dilution through tumor growth, accompanied by low additional CD3xTRP1 accumulation (online supplemental table S2). A similar effect was observed for CD3xMock but not for TRP1xMock which continued to accumulate in KPC3-TRP1 tumors over time. SPECT/CT imaging results of CD3xTRP1 corresponded with the ex vivo biodistribution analyses (figure 3A,C). Additionally, SPECT/CT imaging showed rapid [^{111}In]In-bsAb absorption into the circulation, and uptake in the spleen and KPC3-TRP1 tumor within the first 4 hours following intraperitoneal injection. Lymph node uptake became discernible at 24 hours pi.

These findings were confirmed in B16F10 as a second tumor model, which endogenously expresses TRP1 at approximately fivefold lower levels than the transfected KPC3-TRP1. SPECT/CT and ex vivo biodistribution

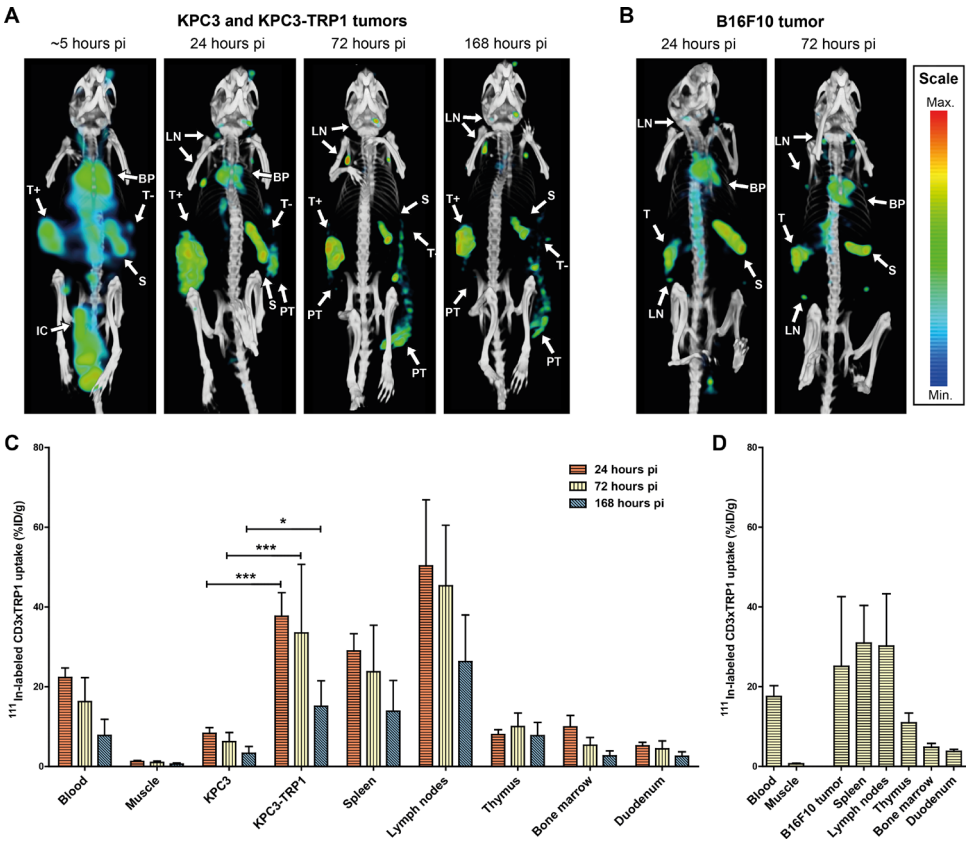

Figure 3 In vivo biodistribution of CD3xTRP1 over time. MicroSPECT/CT and ex vivo biodistribution analyses over time of 12.5 µg [^{111}In]In-CD3xTRP1 intraperitoneally injected C57BL/6J mice bearing either; (1) KPC3-TRP1 and KPC3 tumors on contralateral flanks, or (2) B16F10 tumors. (A) Representative MIPs generated from microSPECT/CT at ~5, 24, 72, and 168 hours pi using the same thresholds visualizing tissue uptake, and (C) the biodistribution at 24, 72, and 168 hours pi of [^{111}In]In-CD3xTRP1in KPC3-tumors bearing mice. (B) Representative MIPs generated from microSPECT/CT at 24 and 72 hours pi using the same thresholds visualizing tissue uptake, and (D) the biodistribution of [^{111}In]In-CD3xTRP1 in B16F10 tumor bearing mice. Indicated tissues on SPECT/CT images: blood pool (BP), intraperitoneal cavity (IC), KPC3-TRP1 tumor (T+), KPC3 tumor (T-), B16F10 tumor (T), spleen (S), lymph nodes (LN), and peri- and extratumoral accumulation (PT). Tissue uptake is presented as %ID/g, differences in uptake were tested for significance using two-way ANOVAs with a Bonferroni post hoc test (*p<0.05, ***p<0.001). ANOVA, analysis of variance; %ID, percentage of the injected dose.

analysis revealed similar pharmacokinetics of [^{111}In]In-CD3xTRP1 (figure 3B,D), but B16F10 tumor uptake was lower than KPC3-TRP1 tumor uptake, although not statistically significant (25.1%ID/g±15.1%ID/g vs 33.5%ID/g±15.4%ID/g, p=ns) (online supplemental table S1). Inguinal lymph node uptake was significantly lower in B16F10 tumor-bearing mice compared with KPC3 tumor-bearing mice (30.2%ID/g±11.3%ID/g vs 45.3%ID/g±13.6%ID/g, p<0.01).

To evaluate whether CD3xTRP1 in circulation was bound to circulating CD3$^+$ cells, we determined the localization of [^{111}In]In-CD3xTRP1 in serum and clotted fractions of blood samples over time. All serum fractions contained ~80% of the radiolabel, suggesting that CD3xTRP1 was generally not bound to CD3$^+$ T cells and presumably available for target binding (online supplemental table S5).

CD3xTRP1 undergoes target-mediated internalization

To investigate the availability of tumor-accumulated and tissue-accumulated CD3xTRP1 for interaction with CD3, we assessed the internalization of CD3xTRP1 by co-administering ^{125}I- and ^{111}In-labeled bsAbs.[23] On bsAb internalization, ^{125}I is released from the cell, while ^{111}In is retained intracellularly. Therefore, the ^{125}I-to-^{111}In ratio provides an estimation of how much accumulated bsAb was internalized. In KPC3-TRP1 tumors, [^{125}I]I-CD3xTRP1 uptake (17.0%ID/g±2.7%ID/g) was significantly lower than [^{111}In]In-CD3xTRP1 uptake at 24 hour pi (37.7%ID/g±5.3%ID/g, p<0.001), resulting in an ^{125}I/^{111}In ratio of 0.45±0.02, meaning that at least 55% of the accumulated CD3xTRP1 was internalized (figure 4, online supplemental table S3 and 4). Significant internalization continued thereafter resulting in approximately 80% of KPC3-TRP1 tumor-accumulated CD3xTRP1 to be unavailable for CD3 interaction at both 72 and 168 hours pi (^{125}I/^{111}In-ratios: 0.22±0.03 and 0.21±0.03). In CD3-rich tissues internalization occurred even faster with 80% of spleen and lymph node accumulated CD3xTRP1 being internalized at 24 hours pi (spleen ^{125}I/^{111}In-ratio: 0.20±0.01). In blood and marker negative tissues, the

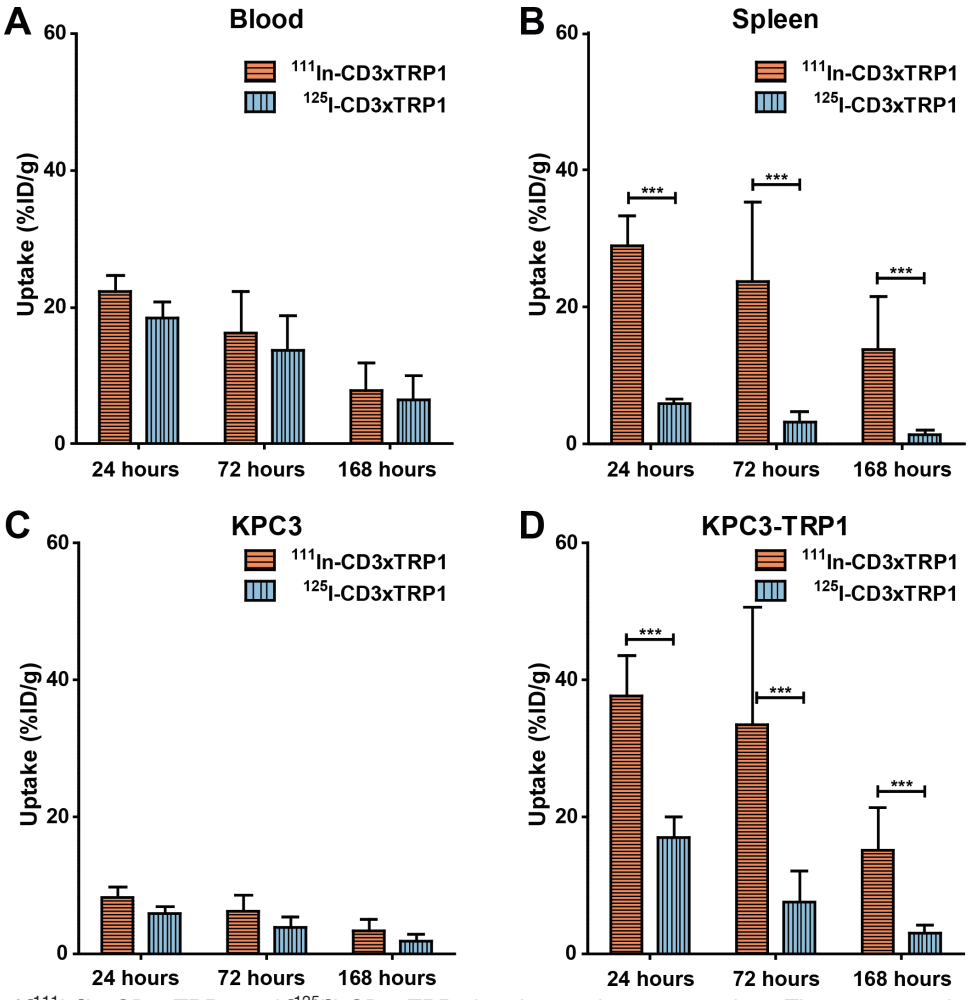

Figure 4 Uptake of [^{111}In]In-CD3xTRP1 and [^{125}I]I-CD3xTRP1 in relevant tissues over time. Tissue accumulation of intracellular residing [^{111}In]In-CD3xTRP1 and cellular effluxing [^{125}I]I-CD3xTRP1 in C57BL/6J mice bearing KPC3-TRP1 and KPC3 tumors that received 12.5 µg of a 1:1 mixture of ^{111}In- and ^{125}I-labeled CD3xTRP1, at 24, 72, and 168 hours post intraperitoneal injection. Blood (A), spleen (B), KPC3 (C), and KPC3-TRP1 (D) tumor uptake are given as %ID/g, differences in uptake were tested for significance using two-way ANOVAs with a Bonferroni post hoc test (***p<0.001). ANOVA, analysis of variance; %ID, percentage of the injected dose.

^{125}I/^{111}In ratio for CD3xTRP1 remained consistent over time, indicating no internalization.

In accordance with its targets, CD3xMock internalization in CD3-rich tissues was similarly high as CD3xTRP1 (online supplemental table S4), whereas the ^{125}I/^{111}In ratios of CD3xMock were comparable in KPC3 and KPC3-TRP1 tumors. Likewise, TRP1xMock internalization in KPC3-TRP1 tumors was similarly high when compared with CD3xTRP1, but considerably lower in CD3-rich tissues. This indicated that internalization of CD3xTRP1 in KPC3-TRP1 tumors and CD3-rich tissues were mostly TRP1- or CD3-mediated. Non-target mediated internalization, however, also occurred as the ^{125}I/^{111}In ratios of CD3xTRP1 and control bsAbs decreased over time in TRP1-negative KPC3 tumors. Additionally, the ^{125}I/^{111}In ratio of TRP1xMock decreased over time in secondary lymphoid organs, indicating internalization through non-specific processes (online supplemental table S4). In summary, CD3xTRP1 rapidly internalized in vivo in KPC3-TRP1 and CD3-rich tissues, this was mostly target-mediated.

CD3xTRP1 reduces KPC3-TRP1 tumor growth and induces immune-cell infiltration

We assessed the therapy effects of a single injection of radiolabeled CD3xTRP1 and control bsAbs by measuring tumor sizes and evaluating the tumor microenvironment for CD3, CD8, Ly6G, F4/80, and PD-L1. KPC3-TRP1 tumors were significantly smaller in mice treated with CD3xTRP1 compared with TRP1xMock at 168 hours pi (mean±SD: 408±170 vs 751±246 mm^3, p<0.05) (figure 5A), whereas KPC3 tumor volumes showed no statistically significant differences. Immunohistochemistry revealed substantial increases in necrotic tumor surface area in CD3xTRP1 treated KPC3-TRP1 tumors. This corresponded with increased CD3$^+$ and CD8$^+$ T-cell numbers in KPC3-TRP1 tumors, as determined by the proportion of CD3-stained or CD8-stained tumor area, which was

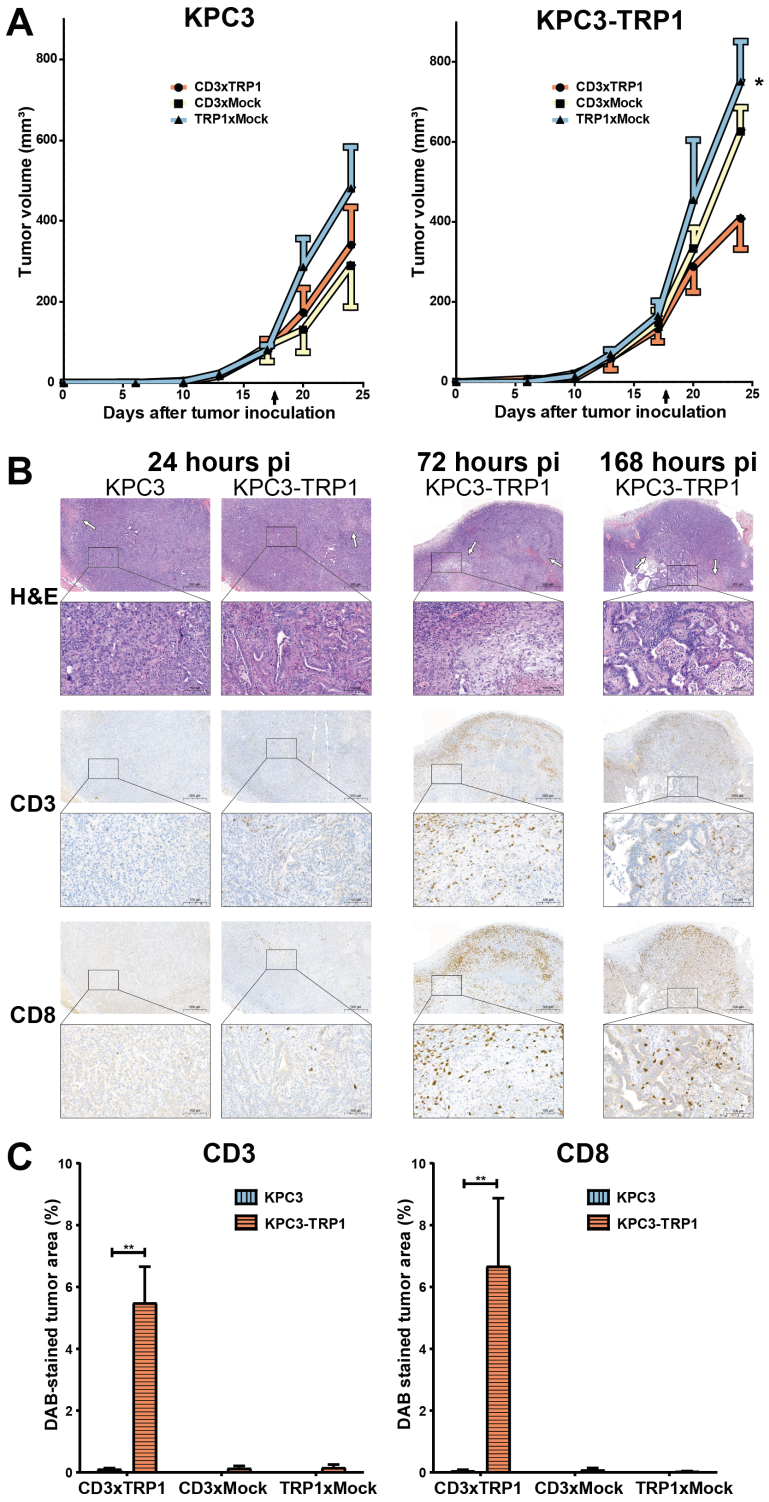

Figure 5 Therapy effects of CD3xTRP1 on KPC3-TRP1 and KPC3 tumors over time. Tumor growth curves and immunohistochemical evaluation of treatment effects in 12.5 µg [^{111}In]In/[^{125}I]I-CD3xTRP1, [^{111}In]In/[^{125}I]I-CD3xMock, and [^{111}In]In/[^{125}I]I-TRP1xMock treated contralateral KPC3 and KPC3-TRP1 tumor-bearing C57BL/6J mice at 24, 72, and 168 hours post intraperitoneal injection. (A) Tumor growth curves of KPC3 and KPC3-TRP1 tumors of radiolabeled CD3xTRP1, CD3xMock, and TRP1xMock treated mice of the 168 hour biodistribution group. Arrow indicates time point of bsAb injection. Data shown are mean±SEM. Differences in KPC3 and KPC3-TRP1 tumor volumes (mean±SD) were tested for significance using one-way ANOVAs with a Bonferroni post hoc test (*p<0.01). (B) Representative images of 5 µm formalin-fixed paraffin-embedded sections of KPC3-TRP1 and KPC3 tumors over time stained for H&E, CD8, and CD3. Arrows indicate necrotic tissue regions. The scale bars represents 500 µm, or 100 µm in insert. (C) Quantified CD3 and CD8 positively stained surface area of KPC3 and KPC3-TRP1 tumors treated with CD3xTRP1, and KPC3-TRP1 treated with CD3xMock, or TRP1xMock, 168 hours pi. Increases in %DAB-stained area were tested for significance using two-tailed t-tests (**p<0.01). ANOVA, analysis of variance; DAB, 3,3'-diaminobenzidine.

most pronounced at 72 hours pi (figure 5B,C, KPC3 vs KPC3-TRP1: 0.11±0.02 vs 5.45±0.95% CD3-DAB-stained area, p<0.01). Furthermore, we observed an increase of neutrophils ($Ly6G^{pos}$) and a shift from a heterogeneous to more homogeneous intratumoral neutrophil distribution in vital KPC3-TRP1 tumor regions (online supplemental figure S4). Additionally, high numbers of $Ly6G^{pos}$ neutrophils and $PD\text{-}L1^{pos}$ cells were observed in necrotic areas. Moreover, $F4/80^{high}$ macrophages surrounded the tumor tissue, while tumor infiltrated macrophages appeared to be $F4/80^{low}$. The number and intratumoral distribution of both $F4/80^{high}$ and $F4/80^{low}$ macrophages did not change over time. Finally, CD3xTRP1 markedly increased membranous PD-L1 expression on KPC3-TRP1 cells on all evaluated time points but most pronounced at 24 and 72 hours pi.

In CD3xMock treated KPC3-TRP1 tumors, the observed effects were substantially less pronounced, with marginally increased necrotic tumor areas, $CD8^+$ T cell numbers, and PD-L1 tumor cell expression only at 24 and 72 hours pi (online supplemental figure S5). In TRP1xMock treated mice all IHC evaluated features were comparable for KPC3-TRP1 and KPC3 tumors. In none of the KPC3 tumors, the effects observed in KPC3-TRP1 tumors were present. In summary, CD3xTRP1 effectuated antitumor immune responses that were predominantly mediated by $CD8^+$ lymphocytes and resulted in necrosis, transient upregulation of PD-L1 on tumor cells, and growth delay in KPC3-TRP1 tumors.

DISCUSSION

Immunotherapeutic CD3-targeting bispecific antibodies cross-link tumor cells with cytotoxic T cells, irrespective of their TCR specificity, thereby inducing local antitumor T-cell responses.[2] To further optimize their efficacy, it is important to understand their pharmacokinetics, uptake in tumor and normal tissues, and cellular internalization. Here, we evaluated these aspects in vivo using a completely syngeneic mouse model consisting of a full-length radiolabeled murine CD3xTRP1 bsAb, immunocompetent mice which endogenously express the TAA, and murine TRP1-expressing tumors. We demonstrate that CD3xTRP1 distributes to TRP1-positive tumors and CD3-positive tissues, and that a large fraction of CD3xTRP1 is internalized. Nonetheless, antitumor immune responses were induced as observed by profound $CD8^+$ T-cell influx and delayed tumor growth.

In vivo pharmacokinetic SPECT/CT imaging and ex vivo biodistribution studies showed that on intraperitoneal administration, CD3xTRP1 is readily absorbed into the circulation, and distributes specifically toward KPC3-TRP1 tumors and CD3-rich tissues, with uptake concentrations peaking 24 hours pi. The following decrease in tumor uptake concentrations was most likely an effect of increasing tumor volume as the absolute tumor uptake, uncorrected for tumor weight, remained constant. In a clinically more relevant tumor model B16F10, with endogenous TRP1 expression levels at approximately fivefold lower than KPC3-TRP1,[10] the tumor uptake of CD3xTRP1 was only twice as low, whereas the overall PK and biodistribution were similar. Although biological differences in tumors, such as vasculature, permeability, and interstitial pressure might differentially affect CD3xTRP1 uptake in these tumor models, these data suggest that TAA expression levels influence the absolute tumor-targeted dose, but not necessarily in a one-to-one correlation.

Our studies with the control bsAb lacking CD3-affinity, together with the initial absence of tumor-residing $CD3^+$ T cells, shows that uptake of CD3xTRP1 in TRP1-positive tumors is primarily TRP1-mediated. It should be noted that CD3xTRP1 treatment resulted in lower KPC3-TRP1 tumor weight compared with control bsAb treatment, which will impact weight-normalized tumor uptake values (%ID/g). However, analyses of the non-normalized data (%ID), did not change the outcome of the study. Circulatory CD3xTRP1 predominantly resided in the serum fraction of blood, indicating that $CD3^+$ T cells are generally not traffickers of CD3-bsAbs to the tumor. In pigmented skin, where endogenous TRP1 is expressed by melanocytes, no measurable specific accumulation of CD3xTRP1 was observed. A potential explanation might be that the localization of melanocytes in the avascular epidermis hinders efficient targeting of CD3xTRP1.[24] This indicates that "on-target, off-tumor" targeting to endogenously expressed TAA does not necessarily affect biodistributions through target-mediated clearance for this bsAb.

Overall, CD3xTRP1's biodistribution is comparable with other CD3-bsAbs that primarily show uptake in lymphoid organs and TAA-expressing tissues.[25 26] For example, in knock-in mice engineered to express human CD3 and the membrane-proximal region of MUC16, the human antibody ^{89}Zr-DFO-REGN4018 recognizing these epitopes showed a highly similar biodistribution pattern compared with our study.[9] However, the uptake of CD3xTRP1 in each organ is consistently lower, which might be explained by variations in the bsAbs affinities, which were undisclosed for REGN4018. Nonetheless, they also showed minimal "on-target, off-tumor" targeting and concluded that the targeting toward the tumor is mainly TAA mediated. This is supportive of the translatability of our findings to the clinical setting. Furthermore, as expected, target-tissue uptake is significantly higher compared with molecules with considerably lower circulatory half-lives, such as bispecific T-cell engagers.[27 28]

SPECT/CT imaging further revealed peritumoral uptake of CD3xTRP1 and control bsAbs around both KPC3 and KPC3-TRP1 but not B16F10 tumors, indicating that it was tumor-type specific and not TRP1- or CD3-mediated. As the Fc-portion of CD3xTRP1 was "LALA" mutated to minimize Fcγ-receptor (FcγR) binding, an FcγR-mediated uptake is also unlikely. However, to definitively exclude FcγRs' involvement a "PGLALA" mutation could be introduced.[29] Therefore, potential explanations for the non-specific uptake include increased angiogenesis

and/or leakiness in the peri-tumoral area, trapping in extracellular matrix deposits induced by tumor cells, or accumulation in extratumoral exudate excreted by the stroma and/or KPC3 cells of pancreatic ductal origin.[14 30]

To exert their therapeutic effect, CD3-bsAbs require simultaneous binding of TAA and CD3 on the membrane of tumor and $CD3^+$ T cells, respectively. Therefore, internalization inevitably decreases its therapeutical available dose. Interestingly, for the therapeutically active CD3xTRP1, we observed receptor-mediated internalization in both KPC3-TRP1 tumors and CD3-rich tissues. In the tumor, this decreased the extracellular dose by half within 24 hours and to ~1/5th within 72 hours pi. In secondary lymphoid organs, even faster internalization resulted in endocytosis of 80% of spleen accumulated CD3xTRP1 within 24 hours. This may be explained by endocytosis signals in CD3ε subunits, which is normally involved in constitutive recycling and down-regulating expression of CD3ε, which can be triggered by T-cell activation and antibody binding.[31 32] Additionally, we observed non-target-mediated internalization of CD3xTRP1, CD3xMock, and TRP1xMock in KPC3 tumors and secondary lymphoid organs, although considerably slower. Possible mechanisms include micropinocytosis, which occurs in T cells and pancreatic ductal adenocarcinomas,[33 34] and phagocytosis of tumor or immune-cell debris by tumor-infiltrated macrophages. Others have also observed internalization of CD3-bsAbs in tumors and secondary lymphoid organs at a fixed 72 hours pi time point using a CD3-bsAb targeting human-CD3ε in transgenic mice expressing both mouse and human CD3ε.[25] We expand on that knowledge by providing a longitudinal overview of this process with our fully functional mouse CD3-bsAb in a non-artificial setting. Previously, on administering CD3xTRP1, transient T-cell activation was observed throughout the body, except for those in the tumor, which stayed activated for at least 4 days.[10] This might be explained by the higher internalization rate in secondary lymphoid organs compared with KPC3-TRP1 tumors, which suggests that balancing CD3-bsAb internalization rates can help mitigate immune related adverse effects (IRAEs), while still inducing prolonged activation of antitumor T-cell responses.

Despite rapidly internalizing, CD3xTRP1 managed to elicit antitumor immune responses as KPC3-TRP1 tumors showed delayed growth, influx of $CD8^+$ T cells, increases in necrotic areas, and a subsequent influx of neutrophils. Thus, the rapidly decreasing non-internalized CD3xTRP1 fraction was apparently sufficient for a therapeutic response. These results correspond with previous findings for CD3xTRP1.[10] Additionally, we observed CD3xTRP1-mediated upregulation of the immune checkpoint PD-L1 on TRP1-positive tumors, which is probably an effect of interferons produced by activated immune cells. This corresponds with previous (pre)clinical observations and thus supports the proposal of combining CD3-bsAbs with immune checkpoint inhibitors to increase antitumor efficacy.[35–37]

Although CD3xTRP1 shows favorable distribution characteristics resulting in effective antitumor immune responses, this study does show opportunities for improving CD3-bsAb immunotherapy by (1) increasing tumor uptake and (2) reducing internalization rates. To increase absolute CD3xTRP1 tumor uptake, shifting uptake from secondary lymphoid organs toward the tumor is preferred above increasing the administered dose as both the tumor and secondary lymphoid organs uptake were not saturated. For high TAA-expressing tumors (eg, KPC3-TRP1) this can be accomplished by decreasing the CD3-affinity of the bsAb, whereas for low TAA expressing-tumors the resulting decrease in therapeutic potency can prohibit this approach.[26 37] Additionally, lowering CD3-affinities may reduce CD3-bsAbs' IRAE potential.[26 38] Other methods to increase tumor uptake include using engineered antibodies formats, such as asymmetric "2-to-1" bsAbs, or using masked CD3-binding arms which are unmasked within the tumor to prevent "on-target, off-tumor" binding.[39] This can also limit activation-induced cell death in secondary lymphoid organs through Abs:CD3-binding, thereby increasing the number of healthy non-anergic T cells that can be recruited for antitumor responses.[40] A second approach to improve CD3-bsAb immunotherapy is through reducing internalization rates. In the tumor, reduced internalization increases the extracellular available dose, thereby mitigating the loss of therapeutic efficacy. This may be accomplished using endocytosis inhibitors, which are currently being developed.[41 42] Another option may be to reduce TAA affinity, as it has been shown that internalization rate increases with epitope affinity for other targets, although contradicting studies exist.[43] In secondary lymphoid organs, when not subsequently retained through subsite rebinding, reduced internalization could result in an increase in CD3-bsAb in circulation, which consequently becomes available for tumor targeting.

Given the many different CD3-bsAb formats that have been developed, which all have different TAA targets, PKs, biodistribution, internalization characteristics, and dosing schedules, it is difficult to provide a clear generalization of our findings to these different formats.[25 26 44] Moreover, secondary lymphoid organs are easily accessible and express large amounts of CD3, therefore they first require target saturation resulting in non-linear pharmacokinetics of CD3-bsAbs. As we investigated a previously determined optimal therapeutic dose (12.5 µg[10]) other doses and effective doses of other CD3-bsAbs might result in different biodistributions, as this is partly determined by the administered dose. All in all, we recommend using preclinical nuclear imaging for clinical CD3-bsAb candidates to obtain insights into key characteristics, such as relative tumor and secondary lymphoid organs targeting and in vivo internalization potency. For studying these human CD3-bsAbs, the use of syngeneic models is preferred to avoid effects such as, transfection-induced differences in TAA expression levels. When artificial models are unavoidable, models closely mimicking

the clinical setting such as human CD3 and human TAA (if applicable) knock-in models are preferred as they still account for their complex immunological interplay with CD3-bsAbs. Then, clinical imaging studies with selected CD3-bsAbs can evaluate their distribution to tumors and healthy tissues, and thus inform on optimal treatment doses, dosing schedules, and the potential for IRAEs.

In summary, we used molecular imaging to assess the pharmacokinetics and biodistribution of CD3xTRP1 bsAb and demonstrate specific and efficient accumulation in both transfected and endogenously TRP1-expressing tumors and CD3-rich tissues in fully syngeneic immunocompetent mice. We further demonstrate that $CD3^+$ T-cell dominated antitumor immune responses can be achieved despite rapid CD3xTRP1 internalization. We are intrigued whether reducing internalization of CD3-bsAbs and/or shifting their uptake toward the tumor can further increase their therapeutic efficacy.

Contributors Conceptualization: GGWS, JM, TVH and SH. Methodology: GGWS, JM, EA, JM-K, TVH and SH. Software: GGWS. Validation: GGWS, JM. Formal analysis: GGWS, JM, JM-K and EW. Investigation: GGWS, JM, EW and JM-K. Resources: JM, TVH and SH. Data Curation: GGWS, JM, EW and JM-K. Writing—original draft preparation: GGWS. Writing—review and editing: GGWS, EW, JM-K, JM, EA, TVH and SH. Visualization: GGWS, JM. Supervision: EA, TVH and SH. Project administration: GGWS, JM. Funding acquisition: TVH and SH. Guarantor: SH.

Competing interests TVH received a research grant from Genmab. Bispecific antibodies were provided by Genmab. TVH and JM are authors on a patent involving the combination of CD3-bsAb therapy in combination with vaccination. The other authors declare that they have no competing interests.

Patient consent for publication Not applicable.

Ethics approval All in vivo experiments and corresponding protocols were approved by the Animal Welfare Body of the Radboud University, Nijmegen, and the Central Authority for Scientific Procedures on Animals (AVD1030020209645) and were performed in accordance with the principles stated by the Dutch Act on Animal Experiments (2014).

Provenance and peer review Not commissioned; externally peer reviewed.

Data availability statement Data are available on reasonable request. Data are available from the authors on reasonable request.

ORCID iDs
Gerwin Gerhard Wemke Sandker http://orcid.org/0000-0002-0997-5440
Erik Aarntzen http://orcid.org/0000-0002-3809-0182
Thorbald van Hall http://orcid.org/0000-0002-9115-558X
Sandra Heskamp http://orcid.org/0000-0001-7250-0846

REFERENCES

1 Dahlén E, Veitonmäki N, Norlén P. Bispecific antibodies in cancer Immunotherapy. *Ther Adv Vaccines Immunother* 2018;6:3–17.
2 Xu H, Cheng M, Guo H, *et al*. Retargeting T cells to Gd2 Pentasaccharide on human tumors using Bispecific Humanized antibody. *Cancer Immunol Res* 2015;3:266–77.
3 Salvaris R, Ong J, Gregory GP. Bispecific antibodies: A review of development, clinical efficacy and toxicity in B-cell Lymphomas. *J Pers Med* 2021;11:355.
4 Tian Z, Liu M, Zhang Y, *et al*. Bispecific T cell Engagers: an emerging therapy for management of hematologic malignancies. *J Hematol Oncol* 2021;14:75.
5 Singh A, Dees S, Grewal IS. Overcoming the challenges associated with Cd3+ T-cell Redirection in cancer. *Br J Cancer* 2021;124:1037–48.
6 Thurber GM, Schmidt MM, Wittrup KD. Antibody tumor penetration: transport opposed by systemic and antigen-mediated clearance. *Adv Drug Deliv Rev* 2008;60:1421–34.
7 Middelburg J, Kemper K, Engelberts P, *et al*. Overcoming challenges for Cd3-Bispecific antibody therapy in solid tumors. *Cancers (Basel)* 2021;13:287.
8 Ellerman D. Bispecific T-cell Engagers: towards understanding variables influencing the in vitro potency and tumor selectivity and their modulation to enhance their efficacy and safety. *Methods* 2019;154:102–17.
9 Crawford A, Haber L, Kelly MP, *et al*. A Mucin 16 Bispecific T cell-engaging antibody for the treatment of ovarian cancer. *Sci Transl Med* 2019;11:eaau7534.
10 Benonisson H, Altıntaş I, Sluijter M, *et al*. Cd3-Bispecific antibody therapy turns solid tumors into inflammatory sites but does not install protective memory. *Mol Cancer Ther* 2019;18:312–22.
11 Labrijn AF, Meesters JI, Bunce M, *et al*. Efficient generation of Bispecific murine antibodies for pre-clinical investigations in Syngeneic rodent models. *Sci Rep* 2017;7:2476.
12 Thomson TM, Mattes MJ, Roux L, *et al*. Pigmentation-associated glycoprotein of human Melanomas and Melanocytes: definition with a mouse Monoclonal antibody. *J Invest Dermatol* 1985;85:169–74.
13 National Library of Medicine. A study of Ro7293583 in participants with Unresectable metastatic Tyrosinase related protein 1 (Tyrp1)-Positive Melanomas. n.d. Available: Clinicaltrials.Gov/show/Nct04551352
14 Hingorani SR, Wang L, Multani AS, *et al*. Trp53R172H and Krasg12D cooperate to promote Chromosomal instability and widely metastatic Pancreatic Ductal adenocarcinoma in mice. *Cancer Cell* 2005;7:469–83.
15 Alegre ML, Tso JY, Sattar HA, *et al*. An anti-murine Cd3 Monoclonal antibody with a low affinity for FC gamma receptors suppresses transplantation responses while minimizing acute toxicity and Immunogenicity. *J Immunol* 1995;155:1544–55.
16 Welt S, Mattes MJ, Grando R, *et al*. Monoclonal antibody to an intracellular antigen images human Melanoma transplants in NU/NU mice. *Proc Natl Acad Sci U S A* 1987;84:4200–4.
17 Zorn JA, Wheeler ML, Barnes RM, *et al*. Humanization of a strategic Cd3 EPITOPE enables evaluation of clinical T-cell Engagers in a fully immunocompetent in vivo model. *Sci Rep* 2022;12:3530.
18 Patel D, Balderes P, Lahiji A, *et al*. Generation and characterization of a therapeutic human antibody to Melanoma antigen Tyrp1. *Hum Antibodies* 2007;16:127–36.
19 Roben P, Moore JP, Thali M, *et al*. Recognition properties of a panel of human recombinant Fab fragments to the Cd4 binding site of Gp120 that show differing abilities to neutralize human immunodeficiency virus type 1. *J Virol* 1994;68:4821–8.
20 Geissler F, Anderson SK, Press O. Intracellular catabolism of Radiolabeled anti-Cd3 antibodies by Leukemic T cells. *Cell Immunol* 1991;137:96–110.
21 Duncan JR, Welch MJ. Intracellular metabolism of Indium-111-DTPA-labeled receptor targeted proteins. *J Nucl Med* 1993;34:1728–38.
22 Sandker GGW, Adema G, Molkenboer-Kuenen J, *et al*. PD-L1 antibody pharmacokinetics and tumor targeting in Mouse models for infectious diseases. *Front Immunol* 2022;13:837370.
23 Boswell CA, Mundo EE, Firestein R, *et al*. An integrated approach to identify normal tissue expression of targets for antibody-drug conjugates: case study of Tenb2. *Br J Pharmacol* 2013;168:445–57.
24 Ryman JT, Meibohm B. Pharmacokinetics of Monoclonal antibodies. *CPT Pharmacometrics Syst Pharmacol* 2017;6:576–88.
25 Mandikian D, Takahashi N, Lo AA, *et al*. Relative target affinities of T-cell-dependent Bispecific antibodies determine Biodistribution in a solid tumor mouse model. *Mol Cancer Ther* 2018;17:776–85.
26 Haber L, Olson K, Kelly MP, *et al*. Generation of T-cell-redirecting Bispecific antibodies with differentiated profiles of cytokine release and Biodistribution by Cd3 affinity tuning. *Sci Rep* 2021;11:14397.

27 Suurs FV, Lorenczewski G, Stienen S, *et al*. The Biodistribution of a Cd3 and Epcam Bispecific T-cell Engager is driven by the Cd3 arm. *J Nucl Med* 2020;61:1594–601.
28 Warnders FJ, Waaijer SJH, Pool M, *et al*. Biodistribution and PET imaging of labeled Bispecific T cell-engaging antibody targeting Epcam. *J Nucl Med* 2016;57:812–7.
29 Schlothauer T, Herter S, Koller CF, *et al*. Novel human Igg1 and Igg4 FC-engineered antibodies with completely abolished immune Effector functions. *Protein Eng Des Sel* 2016;29:457–66.
30 Tian C, Clauser KR, Öhlund D, *et al*. Proteomic analyses of ECM during Pancreatic Ductal adenocarcinoma progression reveal different contributions by tumor and Stromal cells. *Proc Natl Acad Sci U S A* 2019;116:19609–18.
31 Borroto A, Lama J, Niedergang F, *et al*. The Cd3 epsilon subunit of the TCR contains Endocytosis signals. *J Immunol* 1999;163:25–31.
32 Saveanu L, Zucchetti AE, Evnouchidou I, *et al*. Is there a place and role for Endocytic TCR signaling *Immunol Rev* 2019;291:57–74.
33 Michalopoulou E, Auciello FR, Bulusu V, *et al*. Macropinocytosis renders a subset of Pancreatic tumor cells resistant to mTOR inhibition. *Cell Rep* 2020;30:2729–42.
34 Charpentier JC, Chen D, Lapinski PE, *et al*. Macropinocytosis drives T cell growth by sustaining the activation of Mtorc1. *Nat Commun* 2020;11:180.
35 Köhnke T, Krupka C, Tischer J, *et al*. Increase of PD-L1 expressing B-precursor ALL cells in a patient resistant to the Cd19/Cd3-Bispecific T cell Engager antibody Blinatumomab. *J Hematol Oncol* 2015;8:111.
36 Krupka C, Kufer P, Kischel R, *et al*. Blockade of the PD-1/PD-L1 axis augments lysis of AML cells by the Cd33/Cd3 bite antibody construct AMG 330: reversing a T-cell-induced immune escape mechanism. *Leukemia* 2016;30:484–91.
37 Poussin M, Sereno A, Wu X, *et al*. Dichotomous impact of affinity on the function of T cell engaging Bispecific antibodies. *J Immunother Cancer* 2021;9:e002444.
38 Staflin K, Zuch de Zafra CL, Schutt LK, *et al*. Target arm affinities determine Preclinical efficacy and safety of anti-Her2/Cd3 Bispecific antibody. *JCI Insight* 2020;5:e133757.
39 You G, Won J, Lee Y, *et al*. Bispecific antibodies: A smart arsenal for cancer Immunotherapies. *Vaccines (Basel)* 2021;9:724.
40 Dépis F, Hatterer E, Ballet R, *et al*. Characterization of a Surrogate murine antibody to model anti-human Cd3 therapies. *MAbs* 2013;5:555–64.
41 Chew HY, De Lima PO, Gonzalez Cruz JL, *et al*. Endocytosis inhibition in humans to improve responses to ADCC-mediating antibodies. *Cell* 2020;180:895–914.
42 Kaźmierczak Z, Szostak-Paluch K, Przybyło M, *et al*. Endocytosis in cellular uptake of drug delivery vectors: molecular aspects in drug development. *Bioorg Med Chem* 2020;28:S0968-0896(20)30386-2.
43 Rudnick SI, Lou J, Shaller CC, *et al*. Influence of affinity and antigen Internalization on the uptake and penetration of anti-Her2 antibodies in solid tumors. *Cancer Res* 2011;71:2250–9.
44 Nie S, Wang Z, Moscoso-Castro M, *et al*. Biology drives the discovery of Bispecific antibodies as innovative Therapeutics. *Antib Ther* 2020;3:18–62.